

Storage, transport, and fate of perfluoroalkyl acids (PFAAs) in a wastewater re-use and groundwater recharge system

Kalle Jahn¹, Demian M Saffer², Katherine H Freeman³, and Sara Lincoln⁴

¹USGS

²University of Texas at Austin

³Pennsylvania State University

⁴Akima Systems Engineering

December 22, 2022

Abstract

Perfluoroalkyl acids (PFAAs), a group of synthetic compounds associated with adverse human health impacts, are commonly found in effluent discharged from wastewater treatment facilities. When that effluent is used for irrigation, the fate of PFAAs depends strongly on vadose zone solute retention properties and loading history. The relative importance of PFAA retention factors under natural conditions remains uncertain, and the historical record of effluent PFAA concentrations is limited. Using soil cores collected from the Penn State Living Filter (irrigated with treated wastewater effluent for nearly 60 years), we evaluated PFAA transport under near-natural conditions, and estimated historical PFAA concentrations in the irrigated effluent. Total perfluorooctanesulfonic acid (PFOS) and perfluorooctanoic acid (PFOA) masses stored in soils in 2014 were more than 450 times greater than the masses applied during the 2020 effluent irrigation. Equilibrium piston-flow transport models reproduced the observed PFOS and PFOA profiles, allowing us to estimate historical effluent PFOS and PFOA concentrations: 70-170 ng L⁻¹ and 1000-1300 ng L⁻¹, respectively. Estimated concentrations were comparable to concentrations measured in other wastewater effluents in the 1990s and 2000s, indicating that when interpreted with transport modeling, wastewater-irrigated soils function as integrated records of historical PFAA loading. Simulated PFOS breakthrough to groundwater occurred 50 years after the start of wastewater irrigation, while simulated PFOA breakthrough occurred after only 10 years of irrigation. Thus, while wastewater irrigation of soils facilitates retention and reduces effluent PFAA loading to surface waters, the resulting increased PFAA storage in soils potentially creates long-term sources of PFAAs to groundwater.

Hosted file

952264_0_art_file_10540746_rn62b1.docx available at <https://authorea.com/users/568950/articles/614567-storage-transport-and-fate-of-perfluoroalkyl-acids-pfaas-in-a-wastewater-re-use-and-groundwater-recharge-system>

Hosted file

952264_0_supp_10540747_rmydm7.docx available at <https://authorea.com/users/568950/articles/614567-storage-transport-and-fate-of-perfluoroalkyl-acids-pfaas-in-a-wastewater-re-use-and-groundwater-recharge-system>

1 **Storage, transport, and fate of perfluoroalkyl acids (PFAAs) in a wastewater re-**
2 **use and groundwater recharge system**

3 **Kalle L. Jahn^{1†}, Demian M. Saffer^{1,2,3}, Katherine H. Freeman¹, Sara A. Lincoln⁴**

4 ¹ Department of Geosciences, The Pennsylvania State University, University Park, PA, USA

5 ² University of Texas Institute for Geophysics, Jackson School of Geosciences, Austin, TX, USA

6 ³ Department of Geological Sciences, Jackson School of Geosciences, Austin, TX, USA

7 ⁴ Energy and Environmental Sustainability Laboratories, The Pennsylvania State University,
8 University Park, PA, USA

9 Corresponding author: Kalle L. Jahn (kjahn@usgs.gov)

10 †Current address: USGS New York Water Science Center, Troy, New York, USA

11 **Key points**

- 12 • Irrigated soils functioned as records of PFAA loading, and estimated historical effluent
13 PFAA loads were much higher than current loads.
- 14 • Timing of PFAA leaching differed by four decades depending on PFAA sorption affinity.
- 15 • Despite production cessation two decades ago, legacy PFOS stored in vadose zones
16 could remain future source of groundwater contamination.

17

18 **Abstract**

19 Perfluoroalkyl acids (PFAAs), a group of synthetic compounds associated with adverse human
20 health impacts, are commonly found in effluent discharged from wastewater treatment
21 facilities. When that effluent is used for irrigation, the fate of PFAAs depends strongly on
22 vadose zone solute retention properties and loading history. The relative importance of PFAA
23 retention factors under natural conditions remains uncertain, and the historical record of
24 effluent PFAA concentrations is limited. Using soil cores collected from the Penn State Living
25 Filter (irrigated with treated wastewater effluent for nearly 60 years), we evaluated PFAA
26 transport under near-natural conditions, and estimated historical PFAA concentrations in the
27 irrigated effluent. Total perfluorooctanesulfonic acid (PFOS) and perfluorooctanoic acid (PFOA)
28 masses stored in soils in 2014 were more than 450 times greater than the masses applied
29 during the 2020 effluent irrigation. Equilibrium piston-flow transport models reproduced the
30 observed PFOS and PFOA profiles, allowing us to estimate historical effluent PFOS and PFOA
31 concentrations: 70-170 ng L⁻¹ and 1000-1300 ng L⁻¹, respectively. Estimated concentrations
32 were comparable to concentrations measured in other wastewater effluents in the 1990s and
33 2000s, indicating that when interpreted with transport modeling, wastewater-irrigated soils
34 function as integrated records of historical PFAA loading. Simulated PFOS breakthrough to
35 groundwater occurred 50 years after the start of wastewater irrigation, while simulated PFOA
36 breakthrough occurred after only 10 years of irrigation. Thus, while wastewater irrigation of
37 soils facilitates retention and reduces effluent PFAA loading to surface waters, the resulting
38 increased PFAA storage in soils potentially creates long-term sources of PFAAs to groundwater.

39 **1 Introduction**

40 Perfluoroalkyl acids (PFAAs), a group of synthetic and environmentally persistent compounds
41 associated with adverse human health impacts, have been observed in wastewater treatment
42 plant (WWTP) effluent around the world (Chirikona et al., 2015; Gallen et al., 2018; Houtz et al.,
43 2016; Loganathan et al., 2007; Plumlee et al., 2008; Schultz, Higgins, et al., 2006; Sinclair &
44 Kannan, 2006; W. Zhang et al., 2013). There is also evidence that activated sludge treatment
45 processes promote the transformation of polyfluorinated substances to PFAAs, like
46 perfluorooctanoic acid (PFOA) and perfluorooctanesulfonic acid (PFOS), which are not reactive
47 to treatment processes (Hongrui Chen et al., 2017; Sinclair & Kannan, 2006). Wastewater reuse
48 for agricultural irrigation is an important approach to managing treated wastewater, as it
49 reduces both demand on freshwater sources and the volume of treated wastewater discharged
50 to streams. However, if PFAAs are present in the effluent, they can accumulate in the irrigated
51 soils, which can then become long-term sources of PFAAs to groundwater (Brusseau et al.,
52 2019; Guo et al., 2020; Lyu et al., 2018). PFAA-contaminated groundwater is an important and
53 long-term PFAA exposure vector, as groundwater represents 41% of the American total
54 drinking water supply (public and private) and nearly 99% of private single-household drinking
55 water supply (Dieter et al., 2018). The timing and magnitude of PFAA migration from irrigated
56 wastewater to soils, and subsequently to groundwater, depends primarily on the PFAA
57 retention properties of the irrigated soils and the PFAA effluent loading history.

58 The unique molecular structure of PFAAs provides them with several phase-behavior
59 mechanisms for retention in soils, including interaction with organic carbon (Higgins & Luthy,
60 2006), attraction to positively charged mineral surfaces (Hellsing et al., 2016), and accumulation

61 at air-water interfaces (Lyu et al., 2018). Sorption mechanisms are most often studied in
62 laboratory batch and column experiments with concentrated solutions, and there is a dearth of
63 PFAA soil profile data from the field to test the conclusions of these laboratory studies
64 (Brusseau et al., 2020). Additionally, most field studies of PFAA adsorption in vadose zone soils
65 are from sites that received high PFAA loads from aqueous film-forming firefighting foams
66 (Anderson et al., 2019; Bekele et al., 2020; Brusseau et al., 2020; Dauchy et al., 2019). To our
67 knowledge, no field study has investigated PFAA transport and retention in deep soils that have
68 received lower-concentration, decadal-scale irrigation of wastewater effluent.

69 Although waste-water treatment plant (WWTP) discharges account for more than 85% of PFAA
70 releases on continental scales (Sunderland et al., 2019), regular measurements of WWTP
71 effluent PFAA concentrations only began in the mid-2000s (Plumlee et al., 2008; X. Zhang et al.,
72 2017). In industrialized nations, production rates for two common and widely studied PFAAs,
73 Perfluorooctanesulfonic acid (PFOS) and perfluorooctanoic acid (PFOA), increased steadily from
74 the 1970s to peaks in the 1990s before production phase-outs began in 2000 (Paul et al., 2009;
75 Prevedouros et al., 2006). While these production histories have been used to estimate past
76 WWTP discharges (X. Zhang et al., 2017), there are few pre-2000 records of WWTP PFAA
77 concentrations to validate those estimates. This record gap prevents a comprehensive
78 cataloging of the magnitude and distribution of WWTP-derived PFAA contamination of the
79 terrestrial environment.

80 The lack of field studies on PFAA fate in soils and the gaps in PFAA effluent discharge records
81 leave critical unanswered questions about PFAA transport: (1) What soil properties are the best
82 predictors of PFAA transport under natural field conditions? (2) What are the historical PFAA

83 loads on soils irrigated with wastewater effluent? And (3) How long will PFAAs leach from those
84 soils to groundwater if irrigation effluent PFAA concentrations are reduced? These questions
85 have significant human health risk implications.

86 We address these questions using soil cores drilled at a wastewater irrigation spray field as
87 records of both soil PFAA retention behavior and historical PFAA effluent concentrations during
88 >50 years of irrigation. Here, we report correlations between soil properties and PFAA
89 concentrations, and we evaluate PFAA loading and transport history using PFAA mass balances
90 and transport models constrained by site operational history, PFAA production history, and
91 adsorption behavior reported in the literature. In addition to contributing a new record of PFAA
92 retention in deep soils under near-natural conditions, our study illustrates how soil PFAA
93 profiles can be used with simple transport models to estimate historical loading. Model results
94 imply higher PFAA loads in the past and constrain the likely range of historical PFAA
95 concentrations. Our results also suggest that, despite the phase-out of PFOS production in the
96 early 2000s, there is a continued risk of long-term leaching of PFOS from wastewater-irrigated
97 soils due to the highly adsorptive nature of PFOS. Meanwhile, less-adsorptive PFAAs like PFOA
98 have likely already undergone significant leaching to groundwater.

99 **2 Materials and**

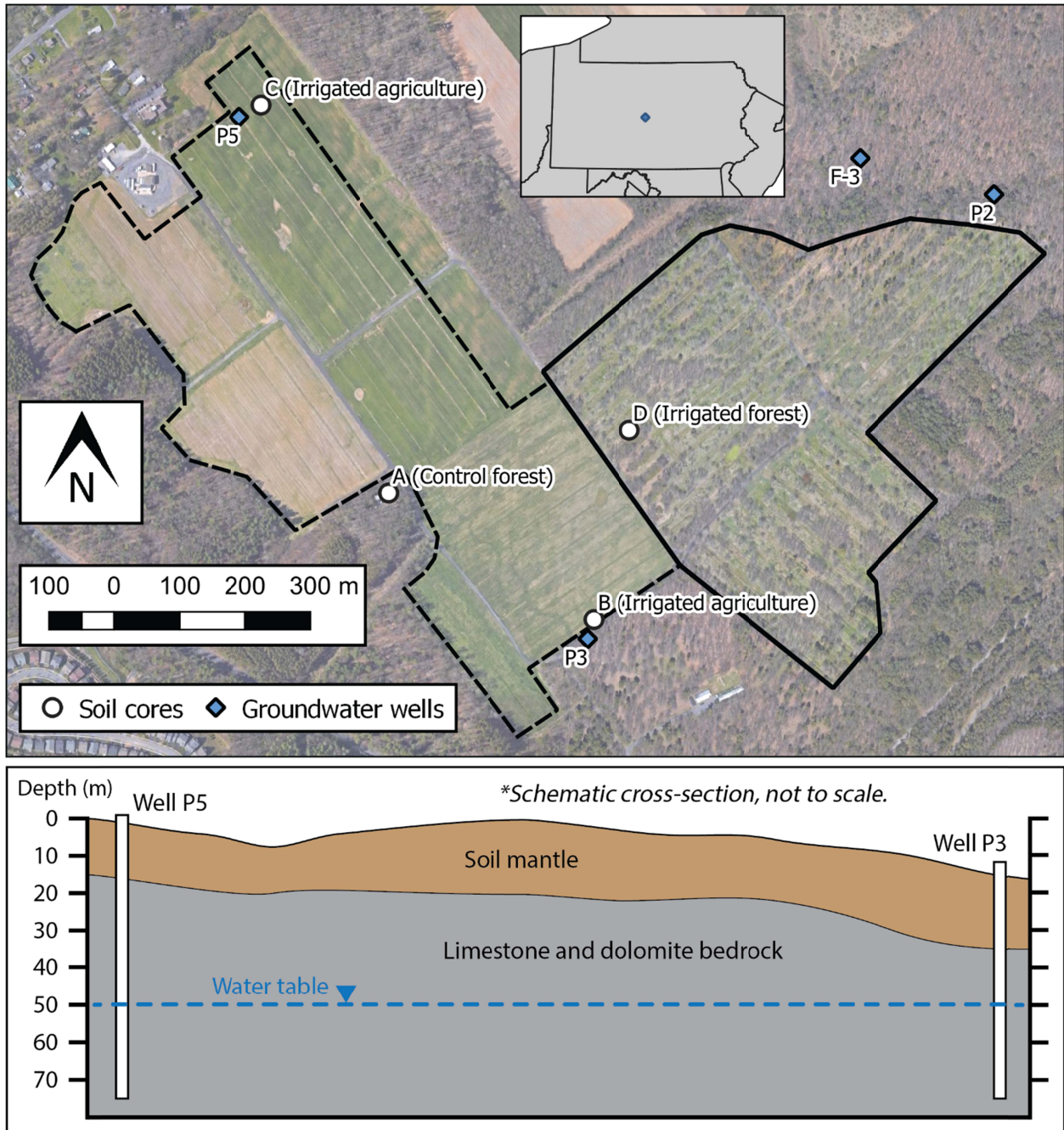
100 This study was conducted at a wastewater reuse site, “The Living Filter,” where treated
101 wastewater is used for irrigation and artificial groundwater recharge. The study focuses on a
102 sub-region of the site, known as “The Astronomy Site,” which has been irrigated continuously
103 since 1964. Effluent from the Penn State University Park Wastewater Treatment Plant is applied
104 at an average annual rate of $\sim 160 \text{ cm yr}^{-1}$ (Walker & Lin, 2008) and precipitation averages ~ 100

105 cm yr⁻¹ (NOAA averages 1981-2010). Irrigation occurs year-round and is typically applied for 12-
106 hours, followed by 6.5-day rest period.

107 The Living Filter is characterized by three different land covers: forest, grasses, and crops. Site
108 soils are predominantly Hagerstown silty clay loam and Hublersburg silt loam, with depths to
109 the underlying limestone and dolomite bedrock as great as 30 m below ground surface (bgs)
110 (Parizek et al., 1967). Soil pH in the top 1 m ranges from 5 to 7, and average saturated hydraulic
111 conductivity in the top 1 m is approximately 2 cm hr⁻¹ (Andrews et al., 2016). Based on depth to
112 groundwater measurements from 2017, 2018, and 2020, depth to groundwater beneath the
113 Astronomy area typically ranges from 20 to 70 m bgs (Ayers et al., 2017; Penn State Office of
114 the Physical Plant, personal communication).

115 The site is underlain by the Cambrian Gatesburg Formation, which locally consists of the Mines
116 Member (coarse-grained dolomite with abundant oolitic chert and thin sandy beds at its base)
117 which overlies the Upper Sandy Member (dolomite with interbedded orthoquartzite and sandy
118 dolomite) (Butts & Moore, 1936; Lattman & Parizek, 1964; Siddiqui & Parizek, 1971; Smith,
119 1969; Wood, 1980). The quartz-rich beds in the Gatesburg can have substantial primary
120 porosity (as great as 20%), while the dolomite-rich beds tend to have porosity <5% (Smith,
121 1969).

122 PFAA concentrations were measured by others in site effluent and groundwater between
123 October 2019 and February 2021 (Mroczo et al., 2022). Four of the groundwater wells
124 sampled were located near the soil core locations at the Astronomy Site (Figure 1), so PFAA
125 concentrations in those wells were used as a constraint on our models.



126

127 Figure 1. Satellite image of the Living Filter Astronomy Area in State College, Pennsylvania.
 128 White circles denote the locations of cores drilled in 2014, blue diamonds denote groundwater
 129 wells sampled for PFAAs in 2020, and black lines denote the area irrigated with treated effluent
 130 (solid for forest and dashed for agricultural land). Total irrigated area is approximately 652,000
 131 m². The schematic cross section below the site map illustrates the approximate range of depths
 132 to bedrock and groundwater between wells P5 and P3.

133 **3 Methods**

134 **3.1 Soil sampling and characterization**

135 Cores were collected as a part of a Master's thesis (Hagedorn, 2016) investigating the fate of
136 nitrate in the Living Filter. The four core locations included: A) a non-irrigated forest site, B) an
137 irrigated cropland topographic depression, C) an irrigated cropland topographic high, and D) an
138 irrigated forest topographic high (Figure 1). At each location, 7.5-cm diameter soil cores were
139 drilled by hydraulic compression in December 2014 and then sampled at ~30 cm intervals.
140 Samples were analyzed for soil bulk density, particle size distributions, mineralogy, and
141 gravimetric water content at the time of drilling. Following the 2014 sampling, the cores were
142 stored at 4°C in a walk-in refrigeration unit at The Pennsylvania State University. In 2019, 42 of
143 the original sample depths were analyzed for PFAAs, total organic carbon, and bulk elemental
144 composition.

145 Dry bulk density was measured by inserting a cylindrical metal tube of known volume into the
146 soil core at the selected depths and weighing that sample following oven drying at 105°C for 24
147 hours. Particle size distributions from 0.06 µm to 880 µm were measured by laser diffraction
148 (Malvern Mastersizer 3000) at the Pennsylvania State University Materials Characterization Lab.
149 Distributions were segregated by Wentworth size classes (clay: <3.9 µm, silt: 3.9-63 µm, sand:
150 63-880 µm) to characterize soil textures. Gravimetric soil water content was calculated by
151 dividing the change in soil sample mass after oven drying (105°C for 24 hours) by the soil dry
152 mass.

153 Iron and aluminum content, intended to function as proxies for relative differences of clay and
154 iron oxide content in the cores, were measured with a handheld x-ray fluorescence (XRF)

155 analyzer (Delta DPO-2000) set to the “Mining Plus” setting and calibrated to a manufacturer-
156 supplied standard. Additionally, 12 samples (samples taken from the top, middle, and bottom
157 of each core) were analyzed for silicate mineralogy by X-ray diffraction (XRD) (Malvern
158 Panalytical Empyrean II). Silicate minerals and their relative abundances were identified from
159 peak angles and intensities using the Rietveld method and the International Centre for
160 Diffraction Data and Inorganic Crystal Structure Database.

161 42 soil samples were analyzed for total carbon (TC) and total organic carbon (TOC) following
162 U.S. Environmental Protection Agency Method 440 (Zimmermann et al., 1997), which is based
163 on carbon mass loss following organic matter combustion. Each soil sample was powdered (<2
164 mm particle diameter) using a mortar and pestle cleaned with methanol and dichloromethane
165 between samples. Each well-mixed powdered sample was sub-sampled into two aliquots, and
166 one aliquot was heated to 550°C in a muffle furnace for 6 hours to combust all organic carbon.
167 Combusted and non-combusted aliquots were then analyzed for TC (wt%) by elemental
168 analyzer (Elementar Vario Max CN) at the Pennsylvania State University Agricultural Analytical
169 Services Laboratory. TOC (wt%) was calculated as the difference between the pre- and post-
170 combustion aliquots (TOC = pre-combustion TC – post-combustion TC). 9 aliquots (3 pre-
171 combustion and 6 post-combustion) were analyzed twice, and the mean TC from the replicates
172 was used to calculate TOC. Standard errors for final TOC values were calculated as the square
173 root of the sum of squared TC standard errors, all of which were less than 5% of the
174 corresponding TOC values. This analytical method may slightly overestimate TOC, as some
175 carbonate minerals can decompose at temperatures below 550°C, though CaCO₃ does not
176 (Zimmermann et al., 1997).

177 Soil samples were analyzed for 32 per- and polyfluoroalkyls (PFASs) by modified EPA method
178 537 Rev 1.1 (Table S1) by Eurofins Lancaster Laboratories (Lancaster, PA). Dry-weight PFAS
179 concentrations were calculated based on soil gravimetric water content at the time of analysis.
180 Matrix spikes were performed to test for matrix suppression of the PFAS signals and labeled
181 isotope recoveries were measured to correct results. PFAS method detection limits (MDL) and
182 limits of quantitation (LOQ) are reported in Table S1. For data analysis, detections between the
183 MDL and LOQ were used quantitatively, and non-detections were treated as equivalent to $\frac{1}{2}$
184 the MDL (Anderson et al., 2019).

185 **3.2 PFAA analyses and profiles**

186 Total PFAA masses stored in the soils below the Living Filter Astronomy spray field were
187 estimated by combining the PFAA results from profiles B, C, and D into an aggregate profile
188 (core A was excluded because it was located outside of the spray field). This representative
189 column was divided into 11 depth intervals (0.0-0.1 m, 0.1-0.25 m, 0.25-0.5 m, 0.5-1 m, 1-2 m,
190 2-3 m, 3-4 m, 4-5 m, 5-6 m, 6-7 m, and 7-8 m). Within each interval, mean PFAA concentrations
191 (ng kg^{-1}) were multiplied by the mean soil bulk density (kg m^{-3}), the interval thickness (m), and
192 the column unit area (1 m^2). The resulting PFAA masses (ng) were summed to obtain total PFAA
193 mass for the soil column (mass per m^2 land surface area). Dividing these total PFAA masses by
194 50 years yielded mean annual rates of PFAA accumulation (mass per m^2 land surface area per
195 year) between the start of effluent application in 1964 and the collection of the cores in 2014

196 **3.3 PFOS and PFOA transport modeling**

197 1-D transport models were developed to gain insight into both historical effluent
198 concentrations and viable field-scale K_{oc} values for soils at the site. The models incorporated

199 both spatial and temporal constraints on the Living Filter system, including the 2014 PFAA soil
200 profiles, 2019-2020 groundwater PFAA concentrations, the Living Filter operational timeline
201 and irrigation rates, and previously compiled global PFAA production and emission trends.
202 Transport modeling was limited to PFOS and PFOA because they are historically the most
203 abundant PFAAs and their production history is better documented than other PFAAs (Paul et
204 al., 2009; Prevedouros et al., 2006).

205 The model domain depth was set to 50 m, close to the 2016-2018 mean groundwater depth
206 under the soil core locations (Ayers et al., 2017; Penn State Office of the Physical Plant,
207 personal communication), as well as groundwater depths in 1963 (Parizek et al., 1967). A
208 column of unit area (1 m^2) was divided into 603 elements with equal pore volume ($\sim 0.03 \text{ m}^3$)
209 (but varying soil mass) defined by using exponential fits to porosity and bulk density profiles
210 from all four cores (Figure S1a and b). For each element, a soil-water adsorption coefficient (K_d)

$$211 \quad K_d = \frac{\text{ng PFAA/kg soil}}{\text{ng PFAA/L water}} \quad (1)$$

212 was calculated using organic carbon fractions (f_{oc}) derived from an empirical fit to TOC data
213 (Figure S1c) and K_{oc} values within the range reported in the literature (Table S2)

$$214 \quad K_d = K_{oc} \times f_{oc} \quad (2)$$

215 Water and PFOA/PFOS were applied in a stepwise fashion to the top element of the model, and
216 then moved from element to element via piston flow. Each applied water volume was equal to
217 the element pore volumes ($\sim 0.03 \text{ m}^3$), corresponding to $\sim 3 \text{ cm}$ of recharge. This volume was

218 equivalent to the mean weekly effluent irrigation rate (3 cm week^{-1}), such that each application
219 represented approximately one week of time.

220 As water and PFOA/PFOS moved through each element, PFOA/PFOS was partitioned between
221 water and the soil of the element as determined by the distribution coefficient K_d . The
222 assumption that concentrations reach equilibrium over the timescale of downward drainage is
223 supported by previous soil and sediment adsorption experiments, which show that as much as
224 ~90% of PFOS and PFOA sorption occurs in less than 10 hours and full adsorption is reached in
225 less than 48 hours (Higgins & Luthy, 2006; Li et al., 2019). The model does not include the
226 production of PFOA/PFOS from the degradation of precursors in the soil column, an assumption
227 that is supported by previous evidence that treatment processes result in substantial
228 transformation of larger precursor compounds to nondegradable PFAAs (Hongrui Chen et al.,
229 2017; Sinclair & Kannan, 2006).

230 PFAA effluent concentrations are unknown for most of the Living Filter operational history, as
231 PFAA concentrations in Living Filter irrigation effluent were first measured in late 2019. While
232 there are no continuous records of treatment plant effluent PFAA concentrations that cover the
233 early 2000s reduction in PFOS and PFOA production, a reduction trend has been recorded a
234 decade later: between 2009 and 2014, mean concentrations of PFOS and PFOA in municipal
235 WWTP effluent discharging into San Francisco Bay decreased by 47% and 34%, respectively
236 (Houtz et al., 2016). Therefore, the PFOS and PFOA production changes in the 2000s likely
237 resulted in commensurate changes in PFOS and PFOA concentrations in wastewater effluent.
238 This same assumption has been made by others developing global emission inventories of PFOS
239 and PFOA (Paul et al., 2009; Prevedouros et al., 2006; X. Zhang et al., 2017), and is also

240 reflected in reductions in PFOS and PFOA in human serum around the world (Sunderland et al.,
241 2019).

242 Based on these previous estimates and observations of PFOS and PFOA historical releases, the
243 post-phase-out change in effluent PFOS and PFOA concentrations at the Living Filter were
244 assumed to occur as a linear decrease between 2000 and 2014 from unknown historical mean
245 concentrations to the effluent concentrations observed in 2020. Although it is a simplification,
246 the 2000-2014 linear reduction in PFOS is supported by the 2012 restriction of PFOS-containing
247 aqueous firefighting foams and the typical 10-year use cycle of PFOS-treated carpets, both of
248 which are significant contributors to PFOS emissions (Paul et al., 2009). The same linear
249 decrease in PFOA is supported by a ~60% reduction in the PFOA parent chemical production
250 between 1999 and 2004 (Prevedouros et al., 2006), and the 2006 PFOA Stewardship Program
251 enacted by the United States Environmental Protection Agency to end PFOA use by 2015
252 (Sunderland et al., 2019).

253 To investigate the PFOS and PFOA loading and adsorption conditions that could produce the
254 2014 profiles, model parameter sweeps were performed to identify best-fitting combinations of
255 K_{oc} and pre-2000 effluent concentrations. The range of K_{oc} was constrained to the range of
256 previously reported K_{oc} values (PFOS: $10^{2.4}$ to $10^{3.8}$ L kg⁻¹, PFOA: $10^{1.9}$ to $10^{2.7}$ L kg⁻¹, see Table S2
257 for referenced studies). Models were evaluated in a two-step process. First, the fit between the
258 simulated 2014 profiles and the observed 2014 profiles was estimated using the root mean
259 square error (RMSE):

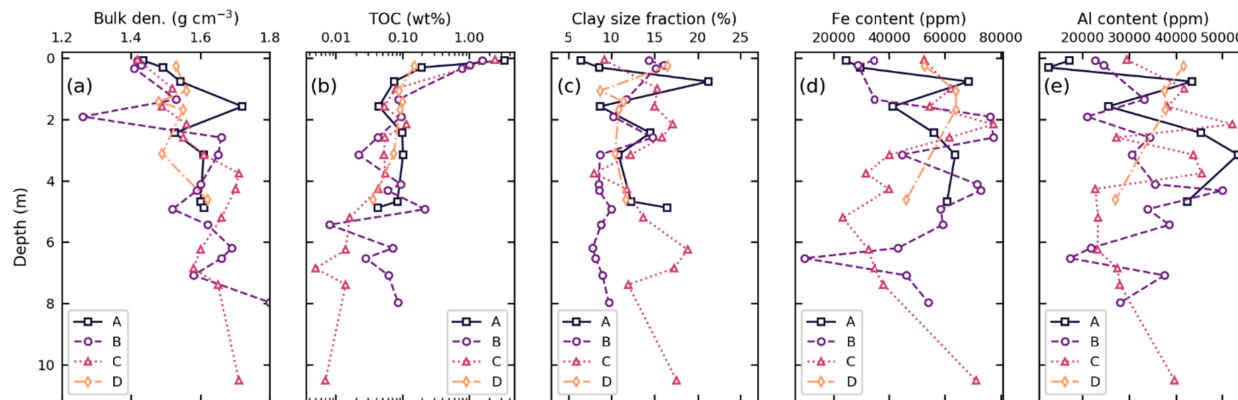
$$260 \quad \text{RMSE} = \sqrt{\frac{1}{N} \sum_{i=1}^N (O_i - S_i)^2} \quad (3)$$

261 where O_i and S_i represent observed and simulated concentrations, respectively. Second, time
262 series of solution concentrations at 30 and 50-m bgs from the low-RMSE models were
263 compared to the mean 2019-2020 PFOS and PFOA groundwater concentrations. The 50-m
264 depth time series was selected based on the mean groundwater depths, and the 30-m depth
265 was used to assess the sensitivity of the time series results to the choice of depth at which soil
266 drainage reaches the water table.

267 **4 Results**

268 **4.1 Soil properties**

269 Variation in bulk density with depth is similar across all four drilling sites, increasing from just
270 over 1.4 g cm^{-3} near the surface to about 1.7 g cm^{-3} at 10.5 m bgs (Figure 2a, Table S3). TOC
271 variation is also similar across all sites, decreasing exponentially with depth from 1-3% in
272 surficial soils to about 0.1% below 1 m bgs (Figure 2b, Table S3 and S4). The exponential
273 decrease in TOC is consistent with previous TOC trends observed at the Living Filter down to 1.2
274 m bgs (Andrews et al., 2016). Clay size fractions are less uniform with depth across the four
275 cores, ranging from 6 to 21%, although mean clay fractions are about the same in all cores (A:
276 12.4%, B: 10.8%, C: 14.1%, D: 11.6%). Iron and aluminum contents generally co-vary, and show
277 a general increasing trend over the top 2-4 m bgs. Based on relative mineral abundances in the
278 XRD data, kaolinite is the dominant clay species across all depths at all four sites (Hagedorn,
279 2016).



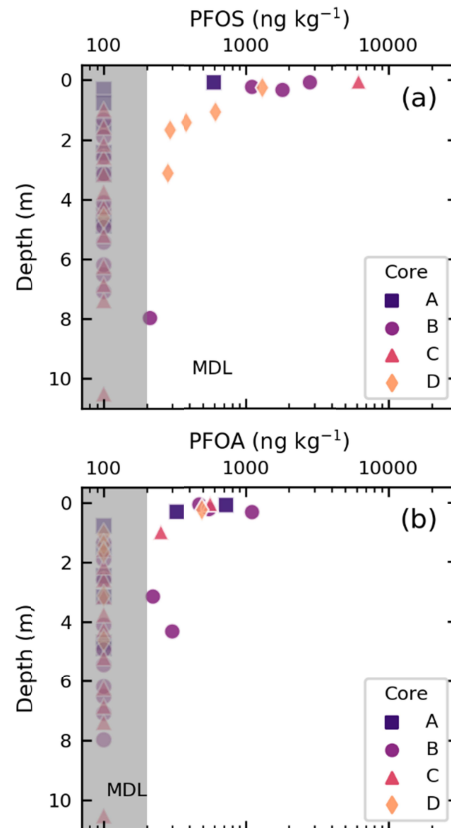
280

281 Figure 2. Depth profiles from the four cores for (a) dry bulk density (g cm^{-3}), (b) total organic
 282 carbon (wt%), clay particle size fraction (volume, %), (d) iron content (ppm by weight), and
 283 aluminum content (ppm by weight)

284 **4.2 PFAA soil profiles and total masses**

285 Only perfluoroalkyl acids (PFAAs) were detected in the soil samples; polyfluoroalkyl compounds
 286 were not detected (Table S5). This corroborates past observations that wastewater treatment
 287 processes (particularly activated sludge) enhance polyfluoroalkyl substance transformation to
 288 PFAAs (Hongrui Chen et al., 2017; Schultz, Higgins, et al., 2006; Sinclair & Kannan, 2006). PFAAs
 289 with chain lengths $> \text{C}_{10}$ were only detected once or twice, mostly in a single near-surface
 290 sample (5 cm bgs in core C). The majority of PFAAs detections were limited to six structures
 291 with carbon chain lengths between C_3 and C_8 (PFBA, PFPeA, PFHxA, PFOA, PFOS, and PFNA, see
 292 Table S1 for full names), so subsequent data analysis focuses on these six PFAAs. When PFAA
 293 depth distributions are aggregated into single profiles, some depth distribution patterns
 294 emerge (Figure 3 and Figure S2). Most PFPeA, PFOA, PFOS, and PFNA detections are confined to
 295 the top 2 m of the profiles, with an apparent exponential decrease with depth. PFBA and PFHxA
 296 distributions also decrease with depth, but with more detections down to 6-8 m bgs than the
 297 longer-chain PFAAs. The PFBA depth distribution in core A, which was an exception to the

298 general decreasing-with-depth pattern, exhibited a steady increase from the surface down to 2-
299 3 m bgs.



300
301 Figure 3. Soil concentration-depth profiles for (a) PFOS and (b) PFOA. Samples are color- and
302 shape-coded by drill site. The sample concentrations that fall below the method detection limit
303 (gray shaded area; MDL < $\sim 200 \text{ ng kg}^{-1}$) are plotted as $\frac{1}{2}$ the method detection limit (MDL) (100
304 ng kg^{-1}).

305 Correlations between PFAA concentrations and soil properties were evaluated using
306 Spearman's and Pearson's correlation coefficients (Table 1). Concentrations of PFAAs with
307 carbon chain length 5 or greater all had significant monotonic and linear positive correlations
308 with TOC ($p < 0.05$), with correlation coefficients generally increasing with chain length (Table
309 1). The lower correlation coefficients between TOC for the shorter-chain PFAAs are consistent
310 with shorter chains having weaker hydrophobic interaction than longer carbon chains. The

311 amount of the shortest chain PFAA (PFBA) was uncorrelated with TOC, but was monotonically
 312 correlated with aluminum and gravimetric water content based on Spearman's coefficient. This
 313 is consistent with a greater importance of electrostatic interactions in the sorption of shorter
 314 chain PFAAs as previously reported (Zhao et al., 2012). Correlation results indicate TOC was the
 315 primary PFAA adsorption control in the Living Filter soils, consistent with the conclusions from
 316 previous studies under both field (Anderson et al., 2019) and laboratory conditions (Higgins &
 317 Luthy, 2006; Li et al., 2019; Milinovic et al., 2015).

318 Table 1. Spearman's and Pearson's correlation coefficients and p-values for six PFAAs and five
 319 soil property metrics. Statistically significant ($p < 0.05$) correlation coefficients are underlined
 320 and bolded.

	PFBA		PFPeA		PFHxA		PFOA		PFOS		PFNA	
Spearman's	rho	p										
TOC	0.11	0.49	<u>0.48</u>	0.00	<u>0.37</u>	0.02	<u>0.53</u>	0.00	<u>0.62</u>	0.00	<u>0.37</u>	0.01
GWC	<u>0.36</u>	0.02	-0.25	0.11	0.10	0.51	-0.13	0.41	0.00	1.00	0.05	0.76
Clay size	0.14	0.38	0.15	0.36	0.02	0.88	-0.06	0.73	-0.02	0.92	0.02	0.90
Al	<u>0.37</u>	0.02	-0.22	0.18	-0.08	0.63	-0.19	0.27	-0.16	0.34	-0.29	0.08
Fe	0.26	0.11	-0.24	0.15	-0.15	0.36	-0.25	0.14	-0.13	0.43	-0.25	0.14
Pearson's	r	p	r	p	r	p	r	p	r	p	r	p
TOC	-0.16	0.31	<u>0.40</u>	0.01	<u>0.38</u>	0.01	<u>0.70</u>	0.00	<u>0.67</u>	0.00	<u>0.44</u>	0.00
GWC	0.12	0.44	-0.18	0.25	0.05	0.77	-0.08	0.61	-0.04	0.82	0.09	0.55
Clay size	0.07	0.67	0.14	0.36	0.06	0.68	0.02	0.91	-0.03	0.85	0.10	0.55
Al	0.29	0.07	-0.21	0.21	-0.04	0.83	-0.26	0.12	-0.13	0.44	-0.20	0.22
Fe	0.15	0.36	-0.19	0.26	-0.13	0.45	-0.27	0.10	-0.07	0.69	-0.12	0.46

321
 322 To evaluate the PFAA masses retained in the Living Filter, total PFAA soil profile masses per m²
 323 land surface area were calculated from aggregated soil profiles (combining cores B, C, and D)
 324 for the four PFAAs with 8 or more detections: PFBA (25445 µg m⁻² land surface area), PFHxA
 325 (2438 µg m⁻²), PFOA (1510 µg m⁻²), and PFOS (2834 µg m⁻²). Assuming consistent irrigation from

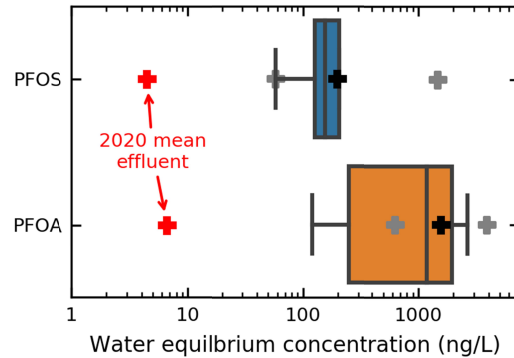
326 1964 through 2014 (50 years), the total masses in the column translate to time-averaged
327 annual soil retention of 509 $\mu\text{g PFBA m}^{-2} \text{ yr}^{-1}$, 49 $\mu\text{g PFHxA m}^{-2} \text{ yr}^{-1}$, 30 $\mu\text{g PFOA m}^{-2} \text{ yr}^{-1}$, and 57
328 $\mu\text{g PFOS m}^{-2} \text{ yr}^{-1}$. With the exception of PFHxA, these values are 2-4 orders of magnitude higher
329 than estimated total PFAA masses applied in 2020 (assuming an irrigation rate of 160 cm yr^{-1}): 9
330 $\mu\text{g PFBA m}^{-2} \text{ yr}^{-1}$, 42 $\mu\text{g PFHxA m}^{-2} \text{ yr}^{-1}$, 11 $\mu\text{g PFOA m}^{-2} \text{ yr}^{-1}$, and 6 $\mu\text{g PFOS m}^{-2} \text{ yr}^{-1}$. This requires
331 that prior to 2014, average effluent PFAA concentrations must have been far higher than
332 measured in 2020.

333 The annually retained masses derived from the mass balance serve as a lower bound on the
334 historical effluent masses: unless dissolved PFAAs were to partition completely to the soil,
335 effluent PFAA masses would have to be higher than the annually retained masses. To provide a
336 conservative estimate of the historical PFAA concentrations needed to produce the observed
337 soil PFOS and PFOA concentrations, we reconstructed equilibrium water concentrations using
338 the soil data. To accomplish this, Equation 2 was used to calculate a K_d value for each soil
339 sample using the relevant sample f_{oc} and the mean K_{oc} value reported in the literature (Table
340 S2). Then, Equation 1 was rearranged to estimate water PFOS and PFOA concentrations from
341 the estimated K_d value and each observed soil concentration under the assumption of
342 equilibrium conditions:

$$343 \quad (\text{ng PFAA/L water}) = (\text{ng PFAA/kg soil}) / K_d \quad (4)$$

344 For PFOS, the mean reported K_{oc} paired with the f_{oc} and PFOS data from 10 soil samples results
345 in 10 estimates of equilibrium water PFOS concentration, with a mean 197 ng L^{-1} and a range of
346 58 to 472 ng L^{-1} (Figure 4). For PFOA, the mean reported K_{oc} paired with data from 8 soil

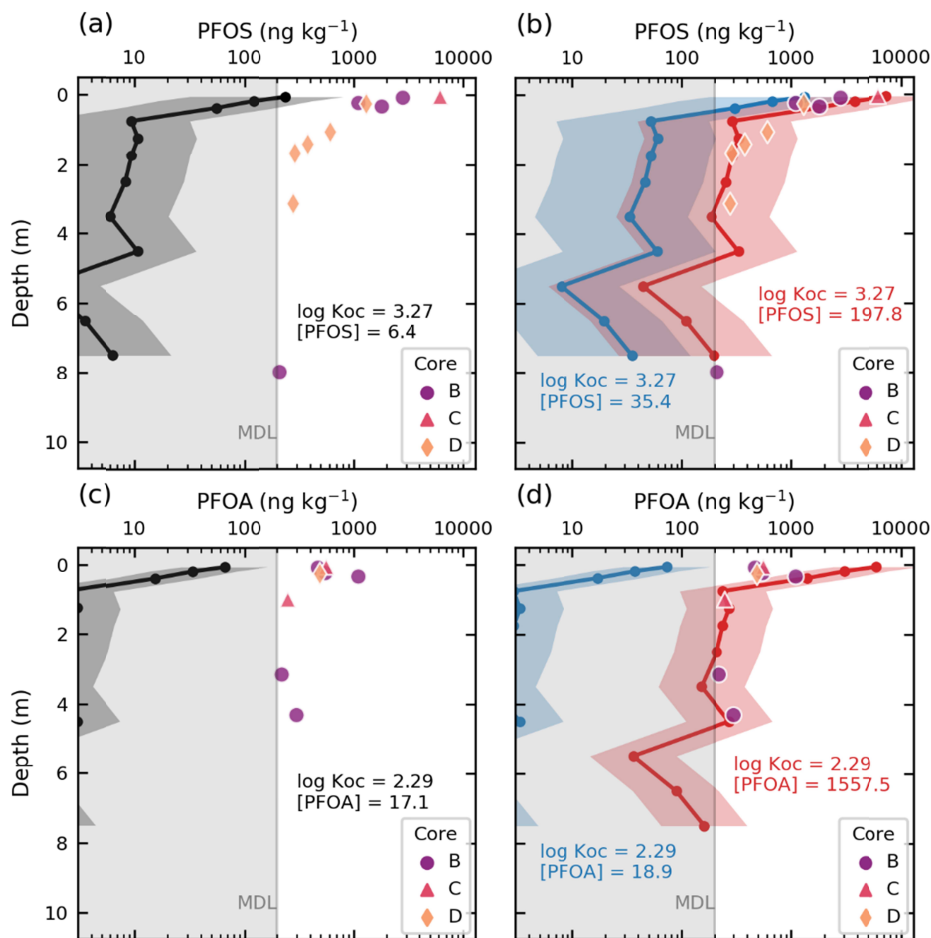
347 samples results in 8 estimates of equilibrium water PFOA concentration, with a mean of 1557
348 ng L^{-1} and a range of 120 to 5183 ng L^{-1} (Figure 4). For both PFOS and PFOA, the lowest values of
349 these ranges are an order of magnitude higher than the 2019-2020 mean effluent
350 concentrations (Figure 4).



351
352 Figure 4. Box plots showing PFOS and PFOA water equilibrium concentrations calculated using
353 Equations 2 and 4 with mean values of reported K_{oc} and soil sample PFOS and PFOA
354 concentrations and organic carbon content. Box edges represent the first and third quartiles,
355 the line through each box represents the median, whiskers show the 10th and 90th percentiles,
356 and the black crosses show the mean equilibrium concentration. The gray crosses show the
357 concentrations calculated using the minimum and maximum reported K_{oc} values, highlighting
358 the variability introduced by the range in literature values. Red crosses show the mean effluent
359 concentrations measured in 2020.

360 To illustrate the PFAA depth distributions that could develop under the three effluent
361 concentration scenarios (1. observed in 2020 effluent, 2. lower bound from mass balance, and
362 3. averaged from an equilibrium assumption), predicted equilibrium profiles were calculated for
363 PFOA and PFOS using the range of previously reported K_{oc} values and soil sample f_{oc} . With the
364 2020 effluent concentrations (PFOS 3.9 ng L^{-1} , PFOA 6.7 ng L^{-1}), predicted PFOS and PFOA
365 equilibrium profiles are as much as one to two orders of magnitude lower than the observed
366 profiles (Figure 5a and c). Using the lower bound for mass balance-derived effluent PFOS
367 concentration (35 ng L^{-1} , PFOA 19 ng L^{-1}), the equilibrium profiles capture some of the observed

368 PFOS concentrations in soils above 0.5 m bgs, but fail to capture the deeper PFOS detections
 369 (Figure 5b). The mass balance-derived effluent PFOA concentration (19 ng L^{-1}) profile remains
 370 approximately an order of magnitude below the observed PFOA concentrations (Figure 5d).
 371 Profiles generated using the third scenario, the average equilibrium concentrations (PFOS 197
 372 ng L^{-1} , PFOA 1557 ng L^{-1} , Figure 4), capture much of the observed PFOS profile (Figure 5b) as
 373 well as the deeper PFOA concentrations, while overpredicting the shallowest soil PFOA
 374 concentrations (Figure 5d).

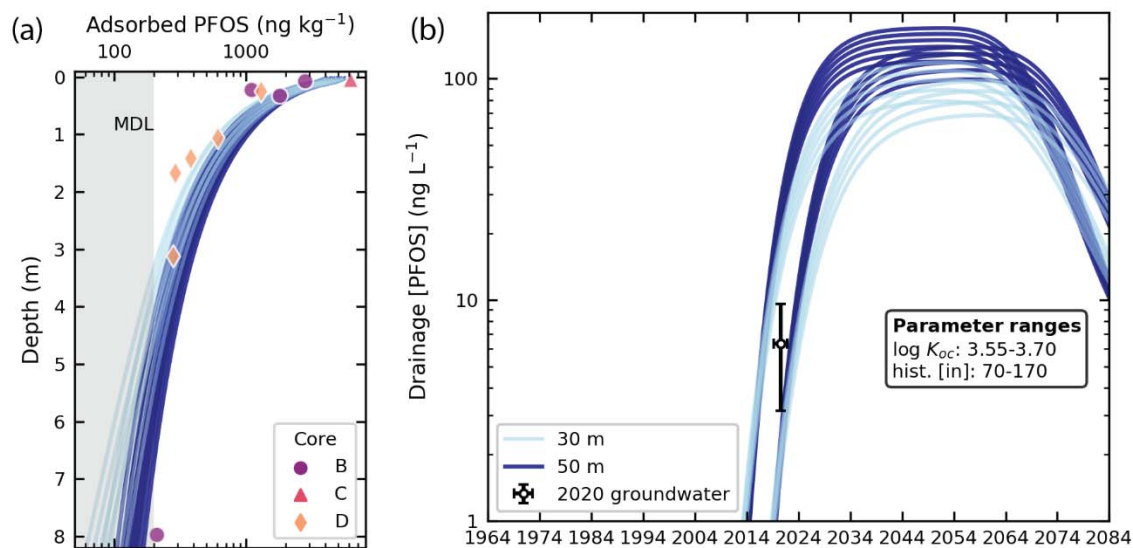


375
 376 Figure 5. Observed PFOS and PFOA concentration profiles from the four Living Filter soil cores
 377 along with theoretical equilibrium profiles. Equilibrium profiles were generated pairing PFOS
 378 and PFOA effluent concentrations ([PFOS] and [PFOA]) with K_d profiles calculated from
 379 measured soil TOC profiles and reported K_{oc} values (lines show the mean K_{oc} and the filled

380 region is bounded by the minimum and maximum reported K_{oc} values). The following effluent
381 concentrations were used: (a) 2020 mean [PFOS] (black line and gray fill), (b) historical mass
382 balance [PFOS] (blue line and fill) and soil-water equilibrium [PFOS] (from Figure 3-4) (red line
383 and fill), (c) 2020 mean [PFOA] (black line and fill), (d) historical mass balance [PFOA] (blue line
384 and fill) and soil-water equilibrium [PFOA] (from Figure 3-4) (red line and fill).

385 4.3 1-D transport models

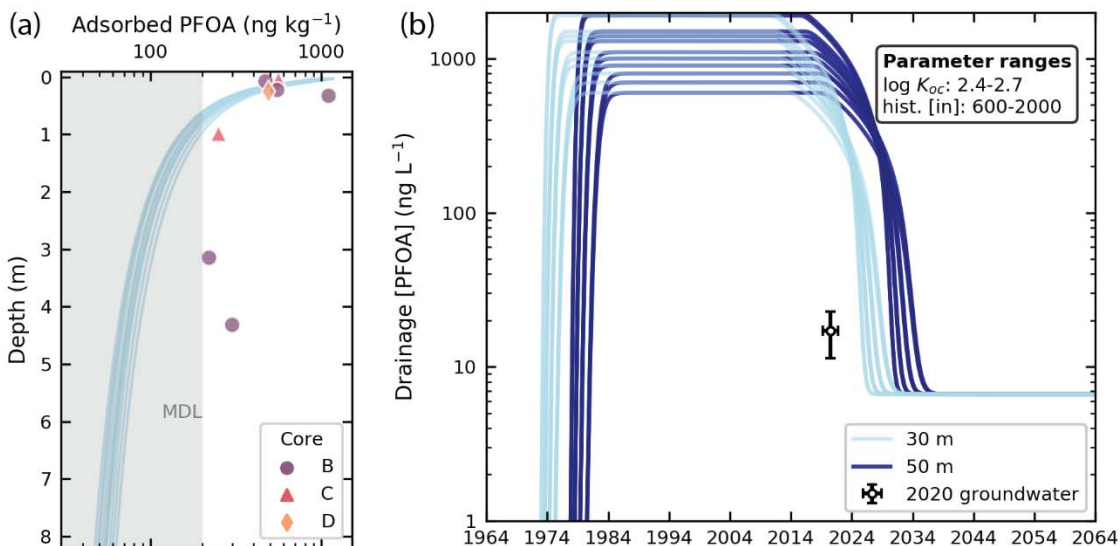
386 For PFOS, cases with historical effluent concentrations between 60 and 180 ng L^{-1} (Figure S3)
387 yielded the best fitting models (those with the lowest RMSE). These required the incorporation
388 of PFOS K_{oc} near the upper bound of reported values ($10^{3.5} - 10^{3.8} \text{ L kg}^{-1}$). A subset of these low-
389 RMSE PFOS transport models also predicted outflow at the base of the soil column consistent
390 with the 2020 groundwater concentrations (Figure 6), with K_{oc} values of $10^{3.55} - 10^{3.7}$, and
391 historical effluent concentrations between 70 and 170 ng L^{-1} .



392
393 Figure 6. Modeling results for PFOS that capture both (a) the 2014 PFOS profile (RMSE < 1100
394 ng kg^{-1}) and (b) the 2020 groundwater PFOS concentration. Predicted concentrations of water
395 draining at the base of the soil column are < 1 ng L^{-1} prior to ~2014.

396 Similarly, the models of PFOA transport with the lowest RMSEs required historical PFOA
397 effluent concentrations between 600 and 2000 ng kg^{-1} (Figure S4) and were limited to those
398 incorporating K_{oc} near the upper bound of values reported in the literature ($10^{2.4} - 10^{2.7} \text{ L kg}^{-1}$).

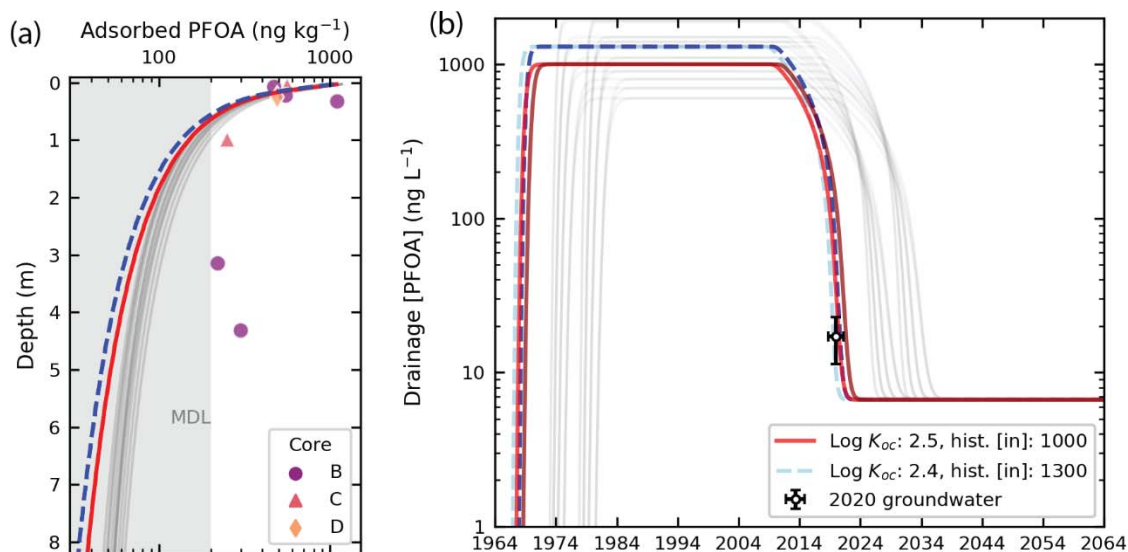
399 None of the models that best fit the 2014 soil PFOA profiles were also able to capture the 2020
400 groundwater concentrations (Figure 7).



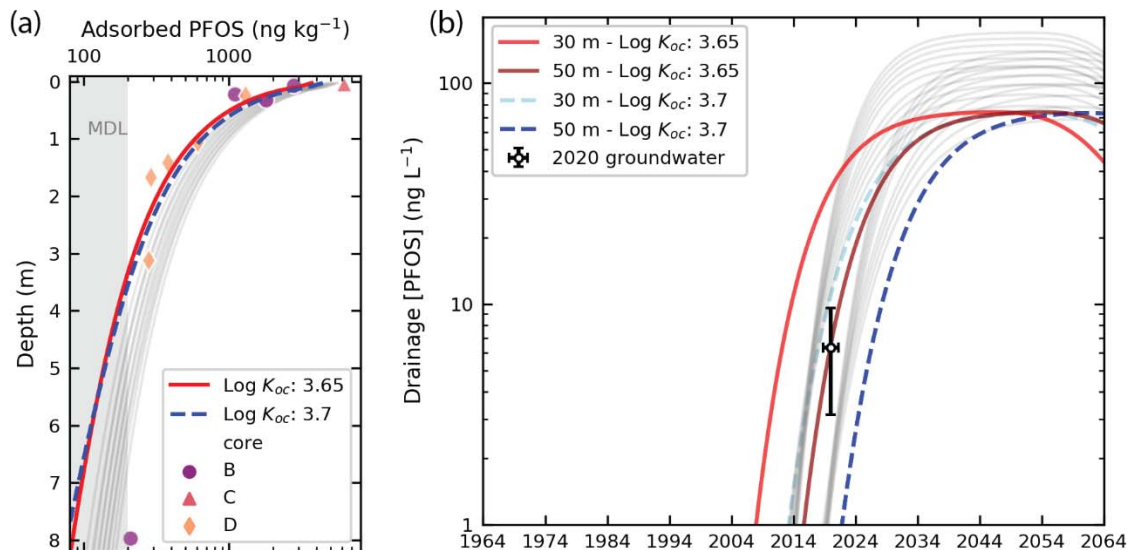
401
402 Figure 7. Modeling results for PFOA that capture both (a) the 2014 PFOA profile (RMSE < 370 ng
403 kg⁻¹). None of these are able to adequately capture (b) the 2020 mean groundwater PFOA
404 concentration.

405 To further explore modeling scenarios that could capture both the 2014 soil profile and 2020
406 groundwater observations without violating the reported range of K_{oc} , we adjusted the PFOA
407 transport model. Specifically, we allowed applied water to percolate through the profile at a
408 higher rate; through seven domain elements per week rather than one, but did not change the
409 rate of surface application. This increased the modeled water flow velocity from ~8 cm per
410 week to ~50 cm per week. The faster-flow model framework successfully captured PFOA
411 profiles and groundwater concentrations while using log K_{oc} values of 2.4 and 2.5, and historical
412 effluent concentrations of 1000 and 1300 ng L⁻¹ (Figure 8). The increased downward flow rate
413 could be accommodated by the Living Filter soils, for which mean saturated hydraulic
414 conductivities are around 2 cm hour⁻¹ (Andrews et al., 2016). The faster flow rate did not

415 drastically alter the outcome of modeled PFOS transport. The faster flow slightly improved the
416 fit to the 2014 PFOS profile, while further constraining the original range of possible K_{oc} and
417 historical concentrations: $\log K_{oc}$ was restricted to between 3.65 and 3.7, and the historical
418 concentration to $\sim 100 \text{ ng L}^{-1}$ (Figure 9).



419
420 Figure 8. Two selected models incorporating a faster water flow rate ($\sim 50 \text{ cm}$ per week rather
421 than $\sim 8 \text{ cm}$ per week) to better capture both constraints on the transport history for PFOA: (a)
422 the 2014 soil profile and (b) the 2020 groundwater concentrations. Shown are cases for depth
423 to groundwater of 30 m (solid red line) and 50 m (solid dark red line), for $K_{oc} = 10^{2.5}$ and
424 historical (pre-2000) concentration of 1000 ng L^{-1} . Also shown are the 30 m (dashed light blue
425 line) and 50 m (dashed dark blue line) time series for $K_{oc} = 10^{2.4}$ and historical mean
426 concentration of 1300 ng L^{-1} . Thin gray lines are the best fitting model results shown in Figure 7.



427
 428 Figure 9. Results from the PFOS transport model incorporating the faster water flow rate (~50
 429 cm per week rather than ~8 cm per week) that better captures transport history for PFOA. A log
 430 K_{oc} of 3.65-6.7 and historical (pre-2000) concentration of 75 ng L⁻¹ best capture both (a) the
 431 2014 soil profile and (b) the 2020 groundwater concentrations. Thin gray lines are the best
 432 fitting PFOS model results shown in Figure 6.

433 Despite the broadly successful model-data comparisons, one locality remained an outlier. None
 434 of the transport simulations were able to match the two PFOA detections in soil samples
 435 collected from core B at 3.1 and 4.3 m bgs. The laboratory-reported PFOA concentration for
 436 sample B-3.1 was on the edge of the laboratory MDL, so the reported value could overestimate
 437 the actual PFOA concentration. Further, the various simulations might not have matched B-4.3
 438 concentration data because of the smoothed f_{oc} data used to define K_d in the model soil
 439 column. This did not capture the highest TOC values, including for B-4.3 (see Figure S1c). The
 440 modelled soil profile therefore underrepresents OC-based PFOA retention for high-TOC depth
 441 intervals in the core. This is evident from the computed PFOA equilibrium profiles (Figure 5),
 442 which do incorporate the detailed depth variability in TOC that was lost in the smoothed fit
 443 used in our modeling, and which capture these higher PFOA concentrations.

444 **5 Discussion**

445 **5.1 PFOS and PFOA adsorption**

446 The K_{oc} values that generated the best fits for both the PFOS and PFOA profiles were consistent
447 with those reported in the literature, but near the upper bound (Table S2). This is consistent
448 with the previously noted trend that field-based studies tend to report higher PFAA K_{oc} values
449 than laboratory studies (Weber et al., 2017; Zareitalabad et al., 2013). Past studies have
450 ascribed this trend to additional sorption factors: 1) interaction with positively charged mineral
451 surfaces, 2) interaction with air-water interfaces, and 3) sorption-desorption hysteresis.

452 The lack of correlations with soil texture, Al content, and Fe content in this study has been
453 observed in other soils (Umeh et al., 2021), even though anion exchange capacity (AEC) does
454 play a role in PFAA adsorption (Li et al., 2019; Umeh et al., 2021). While we did not measure soil
455 AEC, the soil cores had relatively more kaolinite than other clays based on XRD analyses
456 (Hagedorn, 2016). Kaolinite has the highest AEC potential of clays (Radcliffe & Šimůnek, 2010),
457 so the Living Filter soils likely have some capacity to electrostatically retain negatively charged
458 PFAAs. The six detected PFAAs have low pK_a values (Rayne & Forest, 2009), so their head
459 groups will be negatively charged under the Living Filter soil pH range of 5 to 7 (Andrews et al.,
460 2016) and able to interact with positively charged mineral surfaces. However, PFAAs can desorb
461 more easily from mineral surfaces than from organics (Zhao et al., 2012), and PFAAs adsorbed
462 to positively charged alumina plates could easily be removed by gentle rinsing with water.
463 Given that a large amount of water infiltrates through the Living Filter each year ($\sim 260 \text{ cm yr}^{-1}$
464 on average, more than double the average annual precipitation), any adsorption to clays or
465 oxides is probably short-lived.

466 Laboratory column experiments have also shown that PFAA sorption at air-water interfaces
467 (AWI) can greatly enhance PFAA retention in vadose zones (Lyu et al., 2018). While AWI
468 sorption likely occurs at the Living Filter, the soils receive more water than a vadose zone under
469 fully natural conditions (mean annual irrigation of $\sim 160 \text{ cm yr}^{-1}$ in addition to mean annual
470 natural precipitation of $\sim 100 \text{ cm yr}^{-1}$). During collection in December, the soil cores were near
471 saturation, with a mean saturation ratio (soil volumetric water content over porosity) of 0.9.
472 With the frequent irrigation and high soil water content at the Living Filter, it is likely that AWI
473 in the soil profile is highly transient and PFAA retention at AWI is not a significant long-term
474 retention factor.

475 The high K_{oc} values indicated by our modeling could also be field-based evidence for strong
476 PFAA sorption-desorption hysteresis, which has been observed in soil and sediment batch
477 experiments (Huiting Chen et al., 2016; Miao et al., 2017; Milinovic et al., 2015; Zhi & Liu, 2018).
478 Lower desorption yields have been found for PFOS than PFOA, which was ascribed to the higher
479 hydrophobicity of PFOS (Milinovic et al., 2015; Zhao et al., 2012). Notably, Huiting Chen et al.
480 (2016) derived consistently higher PFAA K_{oc} values from desorption experiments, and they
481 suggested sorption irreversibility can result from entrapment of PFAAs within organic matter
482 solids, though the exact process is poorly understood. Sorption irreversibility could be
483 responsible for consistently higher field-based PFAA K_{oc} values compared to lab-based, as
484 speculated by Zareitalabad et al. (2013). Our field-based modeling results appear to support
485 this notion, but there are too few published sorption-desorption data sets to confidently define
486 hysteresis patterns and mechanisms, and the extent of hysteresis may be soil-specific. More
487 work on PFAA sorption-desorption hysteresis is needed in both field and laboratory settings to

488 better define the importance of sorption hysteresis on PFAA retention under natural
489 conditions.

490 **5.2 Historical effluent PFOS and PFOA concentrations**

491 The reduction in global PFOS and PFOA production and use in commercial/industrial products
492 around 2000-2002 suggests that pre-2000 mean effluent concentrations at the Living Filter
493 should be higher than the observed current-day (2020) effluent concentrations. Our simple
494 mass balance analyses confirmed this, and yield required water equilibrium concentrations for
495 PFOS ($197 \pm 41 \text{ ng L}^{-1}$) and PFOA ($1558 \pm 608 \text{ ng L}^{-1}$) significantly higher than the mean 2020
496 effluent concentrations of 3.9 ng L^{-1} and 6.7 ng L^{-1} . Transport modeling informed by the 2014
497 soil profiles in tandem with groundwater data from 2020 further constrained pre-2000 PFOS
498 concentrations to $70 - 170 \text{ ng L}^{-1}$ and pre-2000 PFOA concentrations to around $1000 - 1300 \text{ ng}$
499 L^{-1} .

500 Unfortunately, there are few pre-2000 records of wastewater effluent PFAA concentrations to
501 compare with our model results, especially for WWTPs that do not receive wastewater from
502 PFAA-related industry or manufacture. A 1999 study conducted by 3M measured PFOS and
503 PFOA in six WWTP effluents in the United States, four with known sources of PFAA exposure,
504 and two with no known PFAA sources (Sinclair & Kannan, 2006). One of the two control sites (in
505 Cleveland, TN) had PFOS and PFOA ranges of $417 - 454 \text{ ng L}^{-1}$ and $665 - 674 \text{ ng L}^{-1}$, respectively,
506 and these values are similar to our estimated pre-2000 concentrations. More effluent records
507 are available from the mid-2000s, and while most reported effluent concentrations were below
508 our estimates, some non-industrial WWTPs have comparable PFOS and PFOA concentrations.
509 PFOS concentrations as high as 130 ng L^{-1} were observed in effluent from a Pacific Northwest

510 WWTP treating primarily domestic wastewater (Schultz, Barofsky, et al., 2006). PFOA
511 concentrations as high as 1050 ng L⁻¹ were measured in effluent from New York wastewater
512 treatment plants that treated commercial and domestic wastewater in 2004 and 2005 (Sinclair
513 & Kannan, 2006). Effluent from four California wastewater treatment plants had PFOS and
514 PFOA concentrations that reached 187 ng L⁻¹ and 185 ng L⁻¹ in 2008 (Plumlee et al., 2008).

515 Clearly, pre-2000 effluents with PFOS and PFOA concentrations in the hundreds of ng L⁻¹ have
516 been discharged from WWTPs, with no known PFAA sources in their wastewater streams, and
517 concentrations of similar magnitude have persisted after the PFOS and PFOA production phase-
518 outs. Our pre-2000 effluent estimates lie in comparable ranges, so the Living Filter effluent
519 concentrations estimated in this study align with reasonable loadings of PFAAs over the past
520 three decades.

521 Rain-borne PFOS and PFOA are potential inputs to the Living Filter and were not accounted for
522 in our models. If rainwater or airborne PFAAs are significant sources to the soil and vadose
523 zone, our model estimates would represent overpredictions of past effluent concentrations.
524 However, Scott et al., (2006) measured PFOA concentrations in precipitation across North
525 American between 1998 and 1999, and found that rural areas rarely had PFOA concentrations
526 above 5 ng L⁻¹. Given the rural landscape surrounding the Living Filter, rainfall PFAA
527 contributions to the system were likely insignificant relative to effluent application. If 2020
528 precipitation concentrations were comparable to those measured in the late 1990s,
529 precipitation could represent a PFAA source comparable to the effluent. However, even if
530 1990s precipitation concentrations were subtracted from all modeled effluent concentrations,

531 historical effluent concentrations would still need to be significantly higher than 2020
532 concentrations for the models to match the observed soil profiles.

533 **5.3 Timing of PFOS and PFOA breakthrough and leaching**

534 Because its high K_{oc} , PFOS movement through the soil profile in the best fitting models was
535 significantly retarded, with breakthrough (defined by concentrations $> 1 \text{ ng L}^{-1}$ reaching the
536 base of the soil column as groundwater recharge) only occurring around 2014 (Figure 6b). With
537 the current effluent concentrations and rates of irrigation, future leaching of PFOS from the
538 Living Filter is a distinct possibility. Our models predict that leaching, and concomitantly high
539 PFOS concentrations in recharging groundwater at the base of the soil, will increase for the next
540 ~20 years before reaching a maximum and ultimately beginning to decrease ~60 years after the
541 ramp-down in effluent concentrations (Figure 6b).

542 The rate of leaching will depend on PFOS sorption irreversibility in these soils (lower leaching if
543 high irreversibility), effluent irrigation rates (lower leaching if lower irrigation), and effluent
544 PFOS concentrations (higher leaching if concentrations continue to decrease). While we cannot
545 be certain of the exact timing and magnitudes of PFOS leaching from the Living Filter soils, our
546 modeling effort suggests that the majority of PFOS mass applied over the history of the Living
547 Filter remains stored in soils above the water table. This hypothesis can be tested by collecting
548 additional soil cores and/or by continued monitoring of groundwater concentrations, and
549 would be confirmed if soil PFOS concentrations are still relatively high and groundwater
550 concentrations increase over the coming years. The long-term storage of PFOS in soils is an
551 important consideration for other sites around the world that have received decadal-scale low

552 concentrations of PFOS from wastewater effluent. Even though effluent PFOS concentrations
553 are now low, legacy PFOS loads stored in soils may eventually affect groundwater quality.

554 In contrast, PFOA adsorption sites were saturated more rapidly, and thus more efficient
555 downward transport through the soil column. The best fitting models suggest that
556 breakthrough occurred well before the 2000s, perhaps even within a decade of the start of
557 irrigation (Figure 7b). This was largely because published K_{oc} values suggest organics do not
558 delay PFOA transport to the same degree as PFOS transport. If so, the 2020 groundwater PFOA
559 concentrations are likely not on the rising limb of the breakthrough curve. The observed 2020
560 groundwater concentrations more likely represent the declining limb of the PFOA time series as
561 a result of leaching (Figure 7b). A key implication is that the highest PFOA concentrations
562 leached to groundwater have likely already passed. Similar transport and leaching behavior
563 should be expected for other PFAAs with K_{oc} values comparable to or lower than PFOA, such as
564 PFHxA and PFPeA.

565 The transport model was built with two simplifying assumptions that could impact leaching
566 rates and timing. First, the model assumed water residence times are much longer than the
567 sorption rates of PFOS and PFOA, resulting in equilibrium sorption and aqueous concentrations
568 in pore waters. As discussed above, rapid adsorption has been observed in batch experiments
569 (Higgins & Luthy, 2006; Li et al., 2019). However, breakthrough curves from 1-D column flow
570 interruption experiments indicated rate-limited PFOS sorption under high flow rates (~ 0.4
571 m/day), but showed no evidence for nonequilibrium transport of PFOA (Guelfo et al., 2020). If
572 rate-limited PFOS and PFOA sorption behavior were present under the Living Filter soil
573 conditions, breakthrough could be affected by tailing and rebounding, resulting in longer

574 leaching timeframes and lower peak concentrations than those indicated by our modeling.
575 Second, the transport model represents bulk transport processes and is parameterized with
576 bulk physical and chemical properties collected from the soil cores. Therefore, the model does
577 not capture potential leaching along preferential flow pathways, which would result in the
578 model underestimating the timing and magnitudes of leached PFAA concentrations.

579 The storage and timing of transport illuminated by our analysis raises practical considerations
580 and concerns for wastewater reuse by irrigation. While wastewater irrigation reduces effluent
581 PFAA discharges to surface waters, depending on the production history and sorption behavior
582 of individual PFAAs, wastewater irrigated soils may become long-term sources of PFAAs to
583 groundwater. Even irrigated soils that currently appear to receive very low PFAA loads may
584 have received much higher loads in the past.

585 Collection of soil samples from additional wastewater irrigation sites would allow for
586 corroboration of this outcome and would help the scientific and policy communities assess and
587 validate previously estimated PFAA environmental inventories. In addition to tracking legacy
588 PFAAs like PFOS and PFOA, soils with different wastewater irrigation histories can provide
589 information on the emission histories of newer compounds that replaced PFOS and PFOA, and
590 are not currently regulated. Although TOC-exclusive sorption and piston flow models were
591 satisfactory for testing PFAA transport behavior in this study, future work on these cores and
592 other deep PFAA profiles would benefit from characterizing the impacts of preferential flow
593 and other modes of PFAA soil sorption on transport, and incorporating those factors into more
594 complex reactive transport models.

595 **6 Conclusions**

596 PFAA concentrations were measured in deep soil cores collected from a wastewater effluent
597 spray field. Of the soil properties measured, soil total organic carbon content (TOC) is the best
598 predictor of PFAA distributions in the soil profile, particularly for longer carbon chain PFAAs like
599 PFOS and PFOA. Models of vertical flow, sorption and transport through the soil column yield
600 best-fitting scenarios when K_{oc} is near the upper bound of values reported in the literature, and
601 provide constraints on the time-averaged historical (pre-2000) effluent concentrations. The
602 estimated concentrations are comparable to concentrations measured in some United States
603 WWTP effluents in 1999 and the mid-2000s, indicating that concentrations in soils irrigated
604 with wastewater can be used as records of historical PFAA loading. Even leaching fields that
605 currently receive low PFAA loads may have received higher loads in the past. The model results
606 also indicate stark differences in the leaching timing of PFAAs: the majority of PFOS mass
607 applied over the history of the Living Filter likely remains stored in soils above the water table,
608 while the bulk of the PFOA mass has likely already leached to groundwater. Depending on the
609 production history and sorption behavior of individual PFAAs, wastewater irrigated soils can
610 become a long-term source of PFAAs to groundwater.

611 **7 Acknowledgements**

612 This project was supported by a grant from The Pennsylvania State University Office of the
613 Physical Plant to KJ, DS, and KF. We would like to thank Jake Hagedorn for his collection and
614 original analysis of the cores, which was supported by a grant from The Pennsylvania State
615 University's Sustainability Institute. We thank David Swisher for his input on Living Filter
616 operations. We also thank Roman DiBiase for his insightful review of an early version of the
617 manuscript.

618 **8 Open Research**

619 The data and Python code used for modeling PFAA transport in the study can be found on
620 Zenodo (Jahn, 2022). Python packages used include Matplotlib (Hunter, 2007), NumPy (Harris
621 et al., 2020), Pandas (McKinney, 2010; Reback et al., 2020), Seaborn (Waskom, 2021), and SciPy
622 (Virtanen et al., 2020).

623 **9 References**

- 624 Anderson, R. H., Adamson, D. T., & Stroo, H. F. (2019). Partitioning of poly- and perfluoroalkyl
625 substances from soil to groundwater within aqueous film-forming foam source zones.
626 *Journal of Contaminant Hydrology*, 220, 59–65.
627 <https://doi.org/10.1016/j.jconhyd.2018.11.011>
- 628 Andrews, D. M., Robb, T., Elliott, H., & Watson, J. E. (2016). Impact of long-term wastewater
629 irrigation on the physicochemical properties of humid region soils: “The Living Filter”
630 site case study. *Agricultural Water Management*, 178, 239–247.
631 <https://doi.org/10.1016/j.agwat.2016.10.001>
- 632 Ayers, B., Elkin, K., Kibuye, F., & Gall, H. E. (2017). Pharmaceuticals at Penn State’s Living Filter:
633 From Wastewater to Groundwater. In *2017 Spokane, Washington July 16 - July 19, 2017*.
634 American Society of Agricultural and Biological Engineers.
635 <https://doi.org/10.13031/aim.201700255>
- 636 Bekele, D. N., Liu, Y., Donaghey, M., Umeh, A., Arachchige, C. S. V., Chadalavada, S., & Naidu, R.
637 (2020). Separation and Lithological Mapping of PFAS Mixtures in the Vadose Zone at a
638 Contaminated Site. *Frontiers in Water*, 2, 597810.
639 <https://doi.org/10.3389/frwa.2020.597810>

640 Brusseau, M. L., Yan, N., Van Glubt, S., Wang, Y., Chen, W., Lyu, Y., et al. (2019). Comprehensive
641 retention model for PFAS transport in subsurface systems. *Water Research*, *148*, 41–50.
642 <https://doi.org/10.1016/j.watres.2018.10.035>

643 Brusseau, M. L., Anderson, R. H., & Guo, B. (2020). PFAS concentrations in soils: Background
644 levels versus contaminated sites. *Science of The Total Environment*, *740*, 140017.
645 <https://doi.org/10.1016/j.scitotenv.2020.140017>

646 Butts, C., & Moore, E. S. (1936). *Geology and mineral resources of the Bellefonte quadrangle,*
647 *Pennsylvania* (Geological Survey Bulletin No. 855). U.S. Geological Survey.
648 <https://doi.org/10.3133/b855>

649 Chen, Hongrui, Peng, H., Yang, M., Hu, J., & Zhang, Y. (2017). Detection, Occurrence, and Fate of
650 Fluorotelomer Alcohols in Municipal Wastewater Treatment Plants. *Environmental*
651 *Science & Technology*, *51*(16), 8953–8961. <https://doi.org/10.1021/acs.est.7b00315>

652 Chen, Huiting, Reinhard, M., Nguyen, V. T., & Gin, K. Y.-H. (2016). Reversible and irreversible
653 sorption of perfluorinated compounds (PFCs) by sediments of an urban reservoir.
654 *Chemosphere*, *144*, 1747–1753. <https://doi.org/10.1016/j.chemosphere.2015.10.055>

655 Chirikona, F., Filipovic, M., Ooko, S., & Orata, F. (2015). Perfluoroalkyl acids in selected
656 wastewater treatment plants and their discharge load within the Lake Victoria basin in
657 Kenya. *Environmental Monitoring and Assessment*, *187*(5), 238.
658 <https://doi.org/10.1007/s10661-015-4425-6>

659 Dauchy, X., Boiteux, V., Colin, A., Hémard, J., Bach, C., Rosin, C., & Munoz, J.-F. (2019). Deep
660 seepage of per- and polyfluoroalkyl substances through the soil of a firefighter training

661 site and subsequent groundwater contamination. *Chemosphere*, 214, 729–737.
662 <https://doi.org/10.1016/j.chemosphere.2018.10.003>

663 Dieter, C. A., Maupin, M. A., Caldwell, R. R., Harris, M. A., Ivahnenko, T. I., Lovelace, J. K., et al.
664 (2018). *Estimated use of water in the United States in 2015* (Circular No. 1441) (p. 65).
665 Reston, VA: U.S. Geological Survey. Retrieved from <https://doi.org/10.3133/cir1441>

666 Gallen, C., Eaglesham, G., Drage, D., Nguyen, T. H., & Mueller, J. F. (2018). A mass estimate of
667 perfluoroalkyl substance (PFAS) release from Australian wastewater treatment plants.
668 *Chemosphere*, 208, 975–983. <https://doi.org/10.1016/j.chemosphere.2018.06.024>

669 Guelfo, J. L., Wunsch, A., McCray, J., Stults, J. F., & Higgins, C. P. (2020). Subsurface transport
670 potential of perfluoroalkyl acids (PFAAs): Column experiments and modeling. *Journal of*
671 *Contaminant Hydrology*, 233, 103661. <https://doi.org/10.1016/j.jconhyd.2020.103661>

672 Guo, B., Zeng, J., & Brusseau, M. L. (2020). A Mathematical Model for the Release, Transport,
673 and Retention of Per- and Polyfluoroalkyl Substances (PFAS) in the Vadose Zone. *Water*
674 *Resources Research*, 2019WR026667. <https://doi.org/10.1029/2019WR026667>

675 Hagedorn, J. G. (2016, August). *The Living Filter: monitoring nitrate accumulation after 50 years*
676 *of waster irrigation* (Master of Science). The Pennsylvania State University.

677 Harris, C. R., Millman, K. J., van der Walt, S. J., Gommers, R., Virtanen, P., Cournapeau, D., et al.
678 (2020). Array programming with NumPy. *Nature*, 585(7825), 357–362.
679 <https://doi.org/10.1038/s41586-020-2649-2>

680 Helsing, M. S., Josefsson, S., Hughes, A. V., & Ahrens, L. (2016). Sorption of perfluoroalkyl
681 substances to two types of minerals. *Chemosphere*, 159, 385–391.
682 <https://doi.org/10.1016/j.chemosphere.2016.06.016>

683 Higgins, C. P., & Luthy, R. G. (2006). Sorption of Perfluorinated Surfactants on Sediments.
684 *Environmental Science & Technology*, 40(23), 7251–7256.
685 <https://doi.org/10.1021/es061000n>

686 Houtz, E. F., Sutton, R., Park, J.-S., & Sedlak, M. (2016). Poly- and perfluoroalkyl substances in
687 wastewater: Significance of unknown precursors, manufacturing shifts, and likely AFFF
688 impacts. *Water Research*, 95, 142–149. <https://doi.org/10.1016/j.watres.2016.02.055>

689 Hunter, J. D. (2007). Matplotlib: A 2D Graphics Environment. *Computing in Science &*
690 *Engineering*, 9(3), 90–95. <https://doi.org/10.1109/MCSE.2007.55>

691 Jahn, K. (2022). Storage, transport, and fate of perfluoroalkyl acids (PFAAs) in a wastewater re-
692 use and groundwater recharge system - data and code. Zenodo [Dataset and Software].
693 <https://doi.org/10.5281/zenodo.7439554>

694 Lattman, L. H., & Parizek, R. R. (1964). Relationship between fracture traces and the occurrence
695 of ground water in carbonate rocks. *Journal of Hydrology*, 2(2), 73–91.
696 [https://doi.org/10.1016/0022-1694\(64\)90019-8](https://doi.org/10.1016/0022-1694(64)90019-8)

697 Li, F., Fang, X., Zhou, Z., Liao, X., Zou, J., Yuan, B., & Sun, W. (2019). Adsorption of perfluorinated
698 acids onto soils: Kinetics, isotherms, and influences of soil properties. *Science of The*
699 *Total Environment*, 649, 504–514. <https://doi.org/10.1016/j.scitotenv.2018.08.209>

700 Loganathan, B. G., Sajwan, K. S., Sinclair, E., Senthil Kumar, K., & Kannan, K. (2007).
701 Perfluoroalkyl sulfonates and perfluorocarboxylates in two wastewater treatment
702 facilities in Kentucky and Georgia. *Water Research*, 41(20), 4611–4620.
703 <https://doi.org/10.1016/j.watres.2007.06.045>

704 Lyu, Y., Brusseau, M. L., Chen, W., Yan, N., Fu, X., & Lin, X. (2018). Adsorption of PFOA at the
705 Air–Water Interface during Transport in Unsaturated Porous Media. *Environmental*
706 *Science & Technology*, 52(14), 7745–7753. <https://doi.org/10.1021/acs.est.8b02348>

707 McKinney, W. (2010). Data Structures for Statistical Computing in Python. In *Proceedings of the*
708 *9th Python in Science Conference* (pp. 56–61). Austin, Texas.
709 <https://doi.org/10.25080/Majora-92bf1922-00a>

710 Miao, Y., Guo, X., Dan Peng, Fan, T., & Yang, C. (2017). Rates and equilibria of
711 perfluorooctanoate (PFOA) sorption on soils from different regions of China.
712 *Ecotoxicology and Environmental Safety*, 139, 102–108.
713 <https://doi.org/10.1016/j.ecoenv.2017.01.022>

714 Milinovic, J., Lacorte, S., Vidal, M., & Rigol, A. (2015). Sorption behaviour of perfluoroalkyl
715 substances in soils. *Science of The Total Environment*, 511, 63–71.
716 <https://doi.org/10.1016/j.scitotenv.2014.12.017>

717 Mroczko, O., Preisendanz, H. E., Wilson, C., Mashtare, M. L., Elliott, H. A., Veith, T. L., et al.
718 (2022). Spatiotemporal patterns of PFAS in water and crop tissue at a beneficial
719 wastewater reuse site in central Pennsylvania. *Journal of Environmental Quality*, 51(6),
720 1282–1297. <https://doi.org/10.1002/jeq2.20408>

721 Parizek, R. R., Kardos, L. T., Sopper, W. E., Myers, E. A., Davis, D. E., Farrell, M. A., & Nesbitt, J. B.
722 (1967). *Waste water renovation and conservation* (The Pennsylvania State University
723 Studies No. 23). University Park, Pennsylvania: The Pennsylvania State University.

724 Paul, A. G., Jones, K. C., & Sweetman, A. J. (2009). A First Global Production, Emission, And
725 Environmental Inventory For Perfluorooctane Sulfonate. *Environmental Science &*
726 *Technology*, 43(2), 386–392. <https://doi.org/10.1021/es802216n>

727 Plumlee, M. H., Larabee, J., & Reinhard, M. (2008). Perfluorochemicals in water reuse.
728 *Chemosphere*, 72(10), 1541–1547. <https://doi.org/10.1016/j.chemosphere.2008.04.057>

729 Prevedouros, K., Cousins, I. T., Buck, R. C., & Korzeniowski, S. H. (2006). Sources, Fate and
730 Transport of Perfluorocarboxylates. *Environmental Science & Technology*, 40(1), 32–44.
731 <https://doi.org/10.1021/es0512475>

732 Radcliffe, D. E., & Šimůnek, J. (2010). *Soil Physics with HYDRUS (First)*. Boca Raton, Florida: CRC
733 Press - Taylor & Francis Group.

734 Rayne, S., & Forest, K. (2009). Theoretical studies on the $pK^{\sim a}$ values of perfluoroalkyl
735 carboxylic acids: Chain helicity. *Nature Precedings*.
736 <https://doi.org/10.1038/npre.2009.3829.1>

737 Reback, J., McKinney, W., jbrockmendel, Bossche, J. V. den, Augspurger, T., Cloud, P., et al.
738 (2020, February 5). pandas-dev/pandas: Pandas 1.0.1. Zenodo.
739 <https://doi.org/10.5281/zenodo.3644238>

740 Schultz, M. M., Higgins, C. P., Huset, C. A., Luthy, R. G., Barofsky, D. F., & Field, J. A. (2006).
741 Fluorochemical Mass Flows in a Municipal Wastewater Treatment Facility.
742 *Environmental Science & Technology*, 40(23), 7350–7357.
743 <https://doi.org/10.1021/es061025m>

744 Schultz, M. M., Barofsky, D. F., & Field, J. A. (2006). Quantitative Determination of Fluorinated
745 Alkyl Substances by Large-Volume-Injection Liquid Chromatography Tandem Mass

746 Spectrometry - Characterization of Municipal Wastewaters. *Environmental Science &*
747 *Technology*, 40(1), 289–295. <https://doi.org/10.1021/es051381p>

748 Scott, B. F., Spencer, C., Mabury, S. A., & Muir, D. C. G. (2006). Poly and Perfluorinated
749 Carboxylates in North American Precipitation [†]. *Environmental Science & Technology*,
750 40(23), 7167–7174. <https://doi.org/10.1021/es061403n>

751 Siddiqui, S. H., & Parizek, R. R. (1971). Hydrogeologic Factors Influencing Well Yields in Folded
752 and Faulted Carbonate Rocks in Central Pennsylvania. *Water Resources Research*, 7(5),
753 1295–1312. <https://doi.org/10.1029/WR007i005p01295>

754 Sinclair, E., & Kannan, K. (2006). Mass Loading and Fate of Perfluoroalkyl Surfactants in
755 Wastewater Treatment Plants. *Environmental Science & Technology*, 40(5), 1408–1414.
756 <https://doi.org/10.1021/es051798v>

757 Smith, R. E. (1969). Petrography-Porosity Relations in Carbonate-Quartz System, Gatesburg
758 Formation (Late Cambrian), Pennsylvania. *AAPG Bulletin*, 53.
759 <https://doi.org/10.1306/5D25C609-16C1-11D7-8645000102C1865D>

760 Sunderland, E. M., Hu, X. C., Dassuncao, C., Tokranov, A. K., Wagner, C. C., & Allen, J. G. (2019).
761 A review of the pathways of human exposure to poly- and perfluoroalkyl substances
762 (PFASs) and present understanding of health effects. *Journal of Exposure Science &*
763 *Environmental Epidemiology*, 29(2), 131–147. [https://doi.org/10.1038/s41370-018-](https://doi.org/10.1038/s41370-018-0094-1)
764 0094-1

765 Umeh, A. C., Naidu, R., Shilpi, S., Boateng, E. B., Rahman, A., Cousins, I. T., et al. (2021). Sorption
766 of PFOS in 114 Well-Characterized Tropical and Temperate Soils: Application of

767 Multivariate and Artificial Neural Network Analyses. *Environmental Science &*
768 *Technology*, 55(3), 1779–1789. <https://doi.org/10.1021/acs.est.0c07202>

769 Virtanen, P., Gommers, R., Oliphant, T. E., Haberland, M., Reddy, T., Cournapeau, D., et al.
770 (2020). SciPy 1.0: fundamental algorithms for scientific computing in Python. *Nature*
771 *Methods*, 17(3), 261–272. <https://doi.org/10.1038/s41592-019-0686-2>

772 Walker, C., & Lin, H. S. (2008). Soil property changes after four decades of wastewater
773 irrigation: A landscape perspective. *CATENA*, 73(1), 63–74.
774 <https://doi.org/10.1016/j.catena.2007.09.002>

775 Waskom, M. L. (2021). seaborn: statistical data visualization. *Journal of Open Source Software*,
776 6(60), 3021. <https://doi.org/10.21105/joss.03021>

777 Weber, A. K., Barber, L. B., LeBlanc, D. R., Sunderland, E. M., & Vecitis, C. D. (2017).
778 Geochemical and Hydrologic Factors Controlling Subsurface Transport of Poly- and
779 Perfluoroalkyl Substances, Cape Cod, Massachusetts. *Environmental Science &*
780 *Technology*, 51(8), 4269–4279. <https://doi.org/10.1021/acs.est.6b05573>

781 Wood, C. R. (1980). *Summary groundwater resources of Centre County, Pennsylvania*
782 (Pennsylvania Geological Survey Water Resource Report No. 48) (p. 69). Harrisburg:
783 Pennsylvania Geological Survey.

784 Zareitalabad, P., Siemens, J., Hamer, M., & Amelung, W. (2013). Perfluorooctanoic acid (PFOA)
785 and perfluorooctanesulfonic acid (PFOS) in surface waters, sediments, soils and
786 wastewater – A review on concentrations and distribution coefficients. *Chemosphere*,
787 91(6), 725–732. <https://doi.org/10.1016/j.chemosphere.2013.02.024>

788 Zhang, W., Zhang, Y., Taniyasu, S., Yeung, L. W. Y., Lam, P. K. S., Wang, J., et al. (2013).
789 Distribution and fate of perfluoroalkyl substances in municipal wastewater treatment
790 plants in economically developed areas of China. *Environmental Pollution*, 176, 10–17.
791 <https://doi.org/10.1016/j.envpol.2012.12.019>

792 Zhang, X., Zhang, Y., Dassuncao, C., Lohmann, R., & Sunderland, E. M. (2017). North Atlantic
793 Deep Water formation inhibits high Arctic contamination by continental
794 perfluorooctane sulfonate discharges: North Atlantic PFOS Inputs to the Arctic. *Global
795 Biogeochemical Cycles*, 31(8), 1332–1343. <https://doi.org/10.1002/2017GB005624>

796 Zhao, L., Zhu, L., Yang, L., Liu, Z., & Zhang, Y. (2012). Distribution and desorption of
797 perfluorinated compounds in fractionated sediments. *Chemosphere*, 88(11), 1390–1397.
798 <https://doi.org/10.1016/j.chemosphere.2012.05.062>

799 Zhi, Y., & Liu, J. (2018). Sorption and desorption of anionic, cationic and zwitterionic
800 polyfluoroalkyl substances by soil organic matter and pyrogenic carbonaceous materials.
801 *Chemical Engineering Journal*, 346, 682–691. <https://doi.org/10.1016/j.cej.2018.04.042>

802 Zimmermann, C. F., Keefe, C. W., & Bashe, J. (1997, September). Method 440.0 Determination
803 of Carbon and Nitrogen in Sediments and Particulates of Estuarine/Coastal Waters Using
804 Elemental Analysis, Revision 1.4. U.S. Environmental Protection Agency. Retrieved from
805 https://cfpub.epa.gov/si/si_public_record_report.cfm?Lab=NERL&dirEntryId=309418
806